J Electr Eng Technol.2017; 12(5): 1821-1834
http://doi.org/10.5370/JEET.2017.12.5.1821

ISSN(Print) 1975-0102
ISSN(Online) 2093-7423

PID Controller Tuning using Co-Efficient Diagram method for Indirect Vector Controlled Drive

G.Durgasukumar†, T.Rama Subba Redddy* and B.Pakkiraiah**

Abstract – Medium voltage control applications due to obtain better output voltage and reduced electro-magnetic interference multi level inverter is used. In closed loop control with inverter, the PI controller does not operate satisfactorily when the operating point changes. This paper presents the performance of Co-Efficient diagram PI controller based indirect vector controlled induction motor drive fed from three-level inverter under different operating conditions (dynamic and steady state). The proposed Co-Efficient diagram PI controller based three level inverter significantly reduces the torque ripple compared to that of conventional PI controller. The performance of the indirect vector controlled induction motor drive has been simulated at different operating conditions. For three-level inverter control, a simplified space vector modulation technique is implemented, which reduces the coordinate transformations complications in the algorithms. The performance parameters, torque ripple contents and THD of induction motor drive with three-level inverter is compared under different operating conditions using CDM-PI and conventional PI controllers.

Keywords: Co-Efficient Diagram PI controller (CDM-PI), Indirect vector control, Space vector modulation (SVM), Three-level diode clamped inverter, Performance improvement, Torque ripple

1. Introduction

Indirect vector control is used in induction motor drives for high dynamic and better performance [1]. But the performance of closed loop controlled induction motor drive is largely influenced by the type of speed and current controllers used. Usually, proportional-integral (PI) controller is used due its simplicity. But the tuning of electric drive controller is a complex problem due to the non-linearities of the machines, power converter and controller. The use of proportional integral is acceptable for most of real applications because of its simplicity in architecture [2]. The key of designing a PI controller is to determine control gains, i.e., proportional gain K_p and integral gain K_i [3]. In spite of its wide spread use there exists no generally accepted design method for the controller [4]. System model is necessary for tuning controller coefficients in an appropriate manner. Neglecting some parameters of the mathematical model, controller coefficients cannot be tuned appropriately and does not operate satisfactorily when the operating point changes.

Some work in the area of designing self-tuning, adaptive and robust PSS [5-7] has been reported for achieving better control over wide range of load variations. However, the complexity and/or real-time computational requirement of such controller preclude their use in actual power plants. The CDM standard form is used for choosing the target closed loop characteristic polynomial. Although the CDM results in pretty robust controllers, if there are large uncertainties in the system CDM itself may not be enough to satisfy robust stability and performance requirements. A pole-zero pair is introduced to create extra design freedoms and then a pole-coloring technique [8] to guarantee robust pole assignment. The pole-zero pair is tuned using Genetic Algorithm by minimizing the shift in the closed-loop poles due to perturbations.

A STATCOM based system consisting of PID and fuzzy logic to improve damping for an off shore wind farm with multi machine system [9]. The improvement in the stability of the system is compared with conventional PID controller. A sensor less vector control of permanent magnet synchronous machine with state observer and tracking controller has been presented [10]. In this it estimate the back EMF, speed for a controller in order to achieve linear dynamics throughout the complete operation. In [11], A Linear matrix inequality (LMI) has been developed with PID controllers for discrete time systems to track desired wave in static and dynamic conditions. A matrix equation developed by nodal admittance method is solved by Genetic Algorithm (GA) technique to predetermine the steady-state performance of SPSEIG [12]. A Study on exact tuning of PID controllers for feedback problems has been presented to eliminate the need for graphical and heuristic procedures [13].

An optimized PID controller is developed by using the lozi-map based chaotic algorithm for the load frequency

† Corresponding Author: Dept. of Electrical and Electronic Engineering, VITS, Hyderabad, India. (durgasukumar@gmail.com)
* Dept. of Electrical and Electronic Engineering, VITS, Hyderabad, India. (trsr72@gmail.com)
** Dept. of Electrical and Electronic Engineering, VFSTR University, Guntur, India. (bhupanapatipakkiraiah@gmail.com)
Received: February 23, 2016; Accepted: March 12, 2017

control [14]. Simulation results are compared with other optimization algorithm and obtained better performance with proposed controller. A self-tuning PID controller is developed by using recursive least square (RLS) with linearization has been presented [15]. It reduces the commissioning time and automatically tunes the PID controller by designing the self-tuning controller. An adaptive PID controller is developed to improve the dynamics performance of the power converter [16]. It improves the settling time. But the drawback is it also reduces the output voltage under dynamic conditions. In [17], a space-vector pulse width modulation scheme for an induction motor with open-end windings which uses instantaneous phase reference voltages for the generation of gating signals. A three level fast space vector modulation by applying neuro fuzzy technique is presented [18-19]. Current control scheme and equilibrating voltages in DC-link capacitors of the neutral-point clamped multilevel inverter (NPC-MLI), using an innovative hexagonal space vector hysteresis current control (SVHCC) technique is discussed [20]. The direct modulation strategy of a three-level and five level inverter with self stabilization of the dc link voltage is explained [21]. The effect of dead-time and developing of dead time compensation with self balancing space vector pulse width mod ulated (SVPWM) with a neutral point clamped (NPC) topology is presented [22]. Neuro-Fuzzy based space vector modulation (SVM) technique for voltage source inverter is proposed [23].

In this paper, Co efficient diagram based PID controller for indirect vector control scheme with three- level inverter fed Induction motor drive is presented. The performance of induction motor at different operating conditions is presented. Mathematical modeling and block diagram of induction motor and indirect vector control is introduced in Section-2. In Section-3, CDM-PI controller design is presented. Space Vector Modulation of three level inverter is described in Section-4. Simulation results of Induction motor drive with the proposed and its comparison with conventional controller based system is presented in the Section-5. Experimental validation using dSPACE kit is presented in Section-6. Finally concluding remarks are stated in Section-7. The parameters of motor are given in Appendix.

2. Modeling of Induction Motor and Indirect Vector Control

The mathematical model of a three-phase, squirrel-cage induction motor can be described in stationary reference frame as [17]

$$V_{qs} = (R_s + pL_s)i_{qs} + pL_m i_{qr} \quad (1)$$

$$V_{ds} = (R_s + pL_s)i_{ds} + pL_m i_{dr} \quad (2)$$

$$0 = pL_m i_{qs} - \omega_r L_m i_{ds} + (R_r + pL_r)i_{qr} - \omega_r L_r i_{dr} \quad (3)$$

$$0 = \omega_r L_m i_{qs} + pL_m i_{ds} + \omega_r L_r i_{qr} + (R_r + pL_r)i_{dr} \quad (4)$$

where $\omega_r = \frac{d\theta}{dt}$, $p = \frac{d}{dt}$

Suffix 's' and 'r' represents stator and rotor respectively V_{ds} and V_{qs} are d-q axis stator voltages respectively, i_{ds}, i_{qs} and i_{dr}, i_{qr} are d-q axis stator currents and rotor currents respectively,R_s and R_r are stator and rotor resistances per phase respectively, L_s, L_r are self inductances of stator and rotor and L_m is mutual inductance

Stator and rotor flux linkages can be expressed as in-terms of inductances as

$$\lambda_{qs} = L_s i_{qs} + L_m i_{qr} \quad (5)$$

$$\lambda_{ds} = L_s i_{ds} + L_m i_{dr} \quad (6)$$

$$\lambda_{qr} = L_r i_{qr} + L_m i_{qs} \quad (7)$$

$$\lambda_{dr} = L_r i_{dr} + L_m i_{ds} \quad (8)$$

The electromagnetic torque Te of the induction motor is given by

$$T_e = \frac{3}{2}\left(\frac{p}{2}\right)\left(\lambda_{qr} i_{dr} - \lambda_{dr} i_{qr}\right) \quad (9)$$

The rotor angle θ is estimated using the measured rotor speed ω_r and slip speed ωsl

$$\theta = \int \omega_e dt = \int (\omega_r + \omega_{sl}) dt = \theta_r + \theta_{sl} \quad (10)$$

The total block diagram of the system with current and speed controllers is as shown in the Fig. 1.

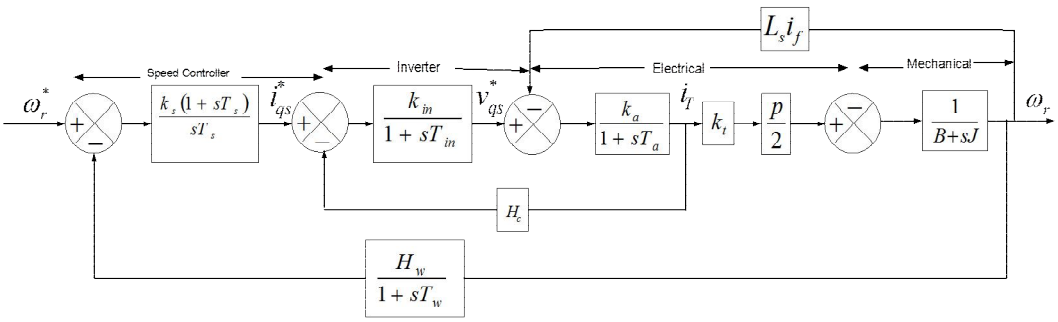

Fig. 1. Block diagram of vector control with speed and current controllers

2.1 Current loop transfer function

From the above overall block diagram vector control the current loop transfer function is

$$(s) = \frac{k_a k_{in}(1+sT_m)}{\{(1+sT_{in})[(1+sT_a)(1+sT_m)+k_a k_b]+H_c k_a k_{in}(1+sT_m)\}} \quad (11)$$

where $k_b = k_m L_s i_f$

$$k_{in} = \frac{p}{2}\frac{k_t}{B}$$

$$T_m = \frac{J}{B}$$

$$T_e = k_t i_T$$

T_{in} is usually negligible compared to T_1, T_2 and T_m
So $1 + sT_{in} = 1$ and

$$(1 + sT_a)(1 + sT_m) \cong (1 + sT_{ar})$$

$$G(s) = \frac{T_1 T_2 K_a K_{in}}{T_{ar} T_m}\frac{1+sT_m}{(1+sT_1)(1+sT_2)} = K\frac{1+sT_m}{(1+sT_1)(1+sT_2)} \quad (12)$$

Where $K = \frac{T_1 T_2 K_a K_{in}}{T_{ar} T_m}$

Where $-\frac{1}{T_1}, -\frac{1}{T_2} = \frac{-b \pm \sqrt{b^2-4ac}}{2a}$

$$a = T_{ar}.T_m$$

$$b = T_{ar} + T_m + H_c K_a K_{in} T_m$$

$$c = 1 + K_a K_b + H_c K_a K_{in}$$

As $T_1 < T_2 < T_m$

$$1 + sT_1 \cong T_1$$

Substituting the above Transfer function is

$$(s) = \frac{K_a k_{in} T_1}{T_{ar}}\frac{1}{(1+sT_1)} = \frac{K_i(1+sT_m)}{(1+sT_2)} \quad (13)$$

Where K_i and T_i are the gain and time constants of simplified current loop

2.2 Speed loop transfer function

The transfer function of closed loop speed controller is

$$G(s) \cong \frac{K_s}{T_s} K_g \frac{(1+sT_s)}{s^2(1+sT_{\omega i})} \quad (14)$$

In the above expression $1+sT_m$ approximated to sT_m and current loop time constant, speed filter time constant are combined into single time constant

$$T_{\omega i} = T_\omega + T_i$$

$$K_g = K_i K_m \frac{H}{T_m}$$

3. Problem Statement

By varying the operating conditions over a wide range which includes almost all practical loading conditions for the motor and by varying the magnitude from very low to high value, so the operating conditions are chosen in the intervals I_d [-0.4 7], I_q [-0.3 5] and ω[2 7]. By taking a step difference of 0.1 in the values of I_d, I_q and ω, totally 300 combinations are obtained which corresponds to 300 operating points.

3.1 PID controllers structure with current loop

Case 1*:* A simple PID-speed and current is considered, when parameters are tuned using standard CDM only. The transfer function of PID is:

$$K(s) = \frac{k_d s^2 + k_p s + k_i}{s} \quad (15)$$

Case 2*:* A PID amended with a pole-zero pair is considered when CDM & pole-coloring are used. The transfer function of vector control with PID is:

$$K(s) = \frac{K_i(1+sT_m)}{(1+sT_2)}\left(\frac{k_d s^2 + k_p s + k_i}{s}\right) \quad (16)$$

The input to is the d and q axis currents, ΔV and the output is ΔU, i.e. $\Delta U = K(s)\,\Delta V$

The parameters of current controller viz. k_d, k_p, k_i, T_i and T_m are tuned through combination of CDM, GA and pole-coloring techniques to meet the desired objectives.

3.1.1 METHOD

a. Concept of CDM:

In CDM, the controllers are designed based on the stability index known as γ_i and the equivalent time constant known as τ which are synthesized from the characteristic polynomial of the closed-loop transfer function.

$$P(s) = a_n s^n + \cdots + a_1 s + a_0 = \sum_{i=0}^{n} a_i s^i \quad (17)$$

From the characteristic polynomial $P(s)$ given in Eq. (17), the stability index γ_i and the equivalent time constant τ are respectively described in general term as the following Eqs. [3]

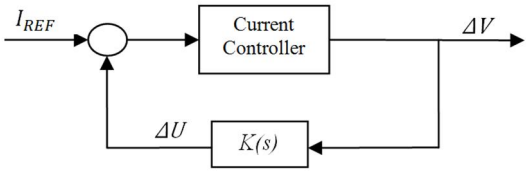

Fig. 2. Closed loop configuration of current controller system

$$\gamma_i = \frac{a_1^2}{a_{i+1}a_{i-1}},\ i = 1{\sim}n-1 \quad (18)$$

$$\tau = \frac{a_1}{a_0} \quad (19)$$

In order to meet the specifications, the equivalent time constant τ and the stability index γ_i are normally chosen as $\tau = \frac{t_s}{2.5} \sim \frac{t_s}{3}\ \gamma_i > 1.5\gamma_i^*$

Where t_s is the specified settling time and γ_i^* is the stability limit defined as

$$\gamma_i^* = \frac{1}{\gamma_{i+1}} + \frac{1}{\gamma_{i-1}}, i = 1{\sim}n-1,\ \gamma_n = \gamma_0 = \infty$$

In general the stability index is recommended as

$$\gamma_{n-1}{\sim}\gamma_2 = 2,\ \gamma_1 = 2.5 \quad (20)$$

known as standard stability index.

Finally the characteristic polynomial known as the desired characteristic polynomial can be expressed as

$$P(s) = a_0\left[\left\{\sum_{i=2}^{n}\left(\prod_{j=1}^{i-1}\frac{1}{\gamma_{i-j}^{j}}\right)(\tau s)^i\right\} + \tau s + 1\right] \quad (21)$$
$$= a_n s^n + \cdots + a_1 s + a_0$$

Where, $a_n, a_{n-1}, \ldots a_0$ are the coefficients of the desired characteristic polynomial.

b. Pole coloring :

Consider the simple case of a third-order system where the nominal poles and perturbed poles for a fixed q (perturbations) are given in Fig. 1. Here, assume that big points represent perturbed poles and small points represent nominal poles corresponds to which of the perturbed poles is called '*pole coloring*'.

c. Graphical approach for checking robustness

Consider a real general polynomial *p(s)* of degree 'n' as given below:

$$p(s) = a_n s^n + a_{n-1}s^{n-1} + \cdots + a_1 s + a_0 \quad (22)$$

The polynomial *p(s)* is said to be an interval polynomial if each coefficient is independent of the other and varies within an interval having a lower and upper bound [5]: i.e. $a_i = [a_i^-, a_i^+],\ i = 0,1,2,\ldots,n.$, such an uncertain polynomial is said to have an independent uncertainty structure.

Kharitonov Theorem: The interval polynomial *p(s)* is robustly stable if and only if the following four Kharitonov polynomials:

$$K_1(s) = a_0^+ + a_1^+ s + a_2^- s^2 + a_3^- s^3 + a_4^+ s^4 + a_5^+ s^5 + \cdots$$
$$K_2(s) = a_0^- + a_1^- s + a_2^+ s^2 + a_3^+ s^3 + a_4^- s^4 + a_5^- s^5 + \cdots$$
$$K_3(s) = a_0^- + a_1^+ s + a_2^+ s^2 + a_3^- s^3 + a_4^- s^4 + a_5^+ s^5 + \cdots$$
$$K_4(s) = a_0^+ + a_1^- s + a_2^- s^2 + a_3^+ s^3 + a_4^+ s^4 + a_5^- s^5 + \cdots \quad (23)$$

are stable [5].

Given the interval polynomial *p(s, a)* as defined in Eq. (7) and a fixed frequency $\omega=\omega_0$, one can describe a set of possible values that $p(j\omega_0, a)$ can assume as *a* varies over the box Q which can be shown as:

$$p(j\omega_0, Q) = \{\, p(j\omega_0, a) : a \in Q\}$$

Then, $p(j\omega_0, Q)$ can be termed as the Kharitonov rectangle [5] at frequency $\omega=\omega_0$ with vertices which are obtained by evaluating the four Kharitonov polynomials, $K_i(s)$, i=1,2,3,4., as defined in equation $s=j\omega_0$. By varying the frequency from $\omega=0$, and with ω increasing in discrete steps, results in the motion of the Kharitonov rectangle with the rectangle moving around the complex plane with vertices $K_i(j\omega)$. The dimensions (size) of this rectangle vary with the frequency *ω*.

Zero Exclusion Condition: Suppose that an interval polynomial family *p(s)* has invariant degree and at least one stable member, the *p(s)* is robustly stable if and only if *s=0* is excluded from the Kharitonov rectangle at all non-negative frequencies [5]; i.e. $0 \notin p(j\omega, Q)$.

The zero exclusion condition suggests a simple graphical procedure for checking robust stability. By watching the motion of Kharitonov rectangle $p(j\omega, Q)$ as ω varies from 0 to +∞, one can easily determine by inspection if the Zero Exclusion condition is satisfied. If it is satisfied, then one can say that the polynomial family *p(s)* is robustly stable.

3.1.2 Controller design

A family of 330 linearized models of the system is constructed for drive with operating points as I_d, I_q and ω vary independently in steps of 0.01 over the interval [-0.4 7], [-0.3 5] and [2 7] respectively. The reference terminal voltage is kept as $\Delta V_{REF}=0.8$ and moment of inertia is calculated as M=2. Open loop poles location: when I_d, I_q and *V* are varied independently in steps of 0.01 over the above interval are shown in Fig. 3.

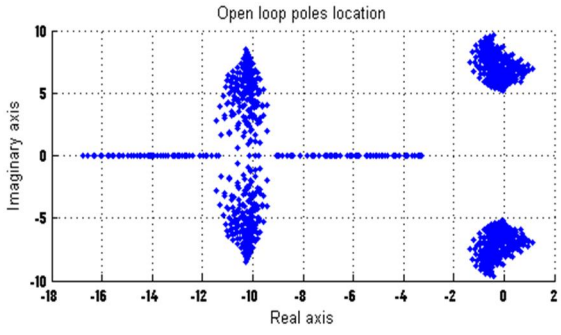

Fig. 3. Open loop poles locations for all chosen perturbations

a) Designing a robust PID:

Step 1. Let the normal loading condition and the nominal operating point, the corresponding transfer function will be

$$G_{light}(s) = \frac{-44.3s}{s^4 + 21.1s^3 + 170.6s^2 + 1102.3s + 4371}$$

Step 2. Choose controller to be designed as PID

Step 3. Obtain the closed loop characteristic polynomial in terms of unknown controller parameters-

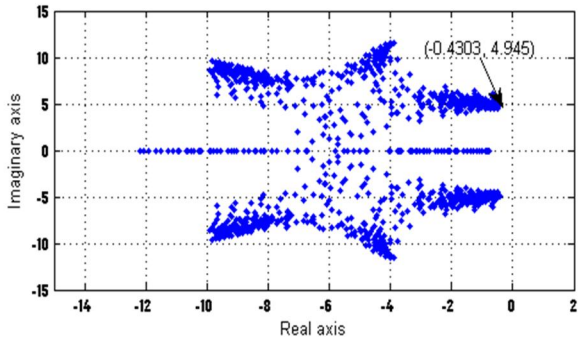

(a)

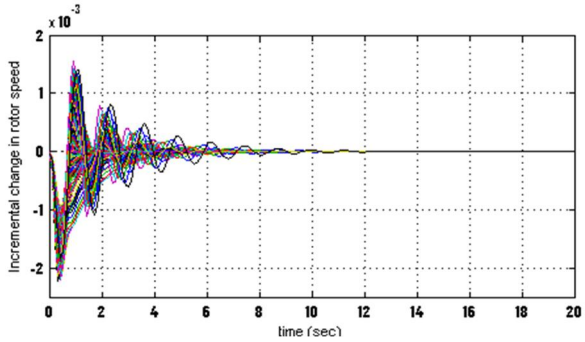

(b)

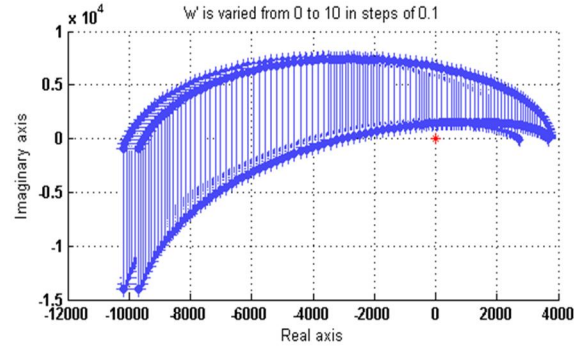

(c)

Fig. 4. (a) Closed-loop poles location. Most dominant pole at -0.43, Minimum damping ratio offered 5°; (b) Closed loop response to a 5% disturbance step at all 300 operating points with k_d =1.1916, k_p =1.7636, k_i=-42.3410; (c) The Kharitonov Rectangles satisfying zero exclusion condition

$$P(s) = s^4 + 21.1s^3 + (170.6s^2 + 44.3k_d)s^2 + (1102.3 + 44.3k_p)s + (4371 + 44.3k_i)$$

$$a_i = [a_5\ a_4\ a_3\ a_2\ a_1\ a_0] = [1\ 21.1\ (170.6s^2 + 44.3k_d)\ (1102.3 + 44.3k_p)\ (4371 + 44.3k_i)] \quad (24)$$

Step 4. Choose the stability indices according to the CDM standard form Eq. (18).

As we have taken γ_i from standard form, stability conditions are satisfied, $\gamma_2 > \gamma_2^*$ from R-H criterion $a_2 > \left(\frac{a_1}{a_3}\right)a_4 + \left(\frac{a_3}{a_1}\right)a_0$ is also satisfied.

Step 5. From equations (18), (20) & (24), k_d=1.1916, k_p = 1.7636, ki = -42.3410.

The interval characteristic polynomial of the closed loop system becomes:

$$G^I_{interval} = [1,1]s^4 + [20.66, 21.13]s^3 + [229.22, 233.84]s^2 + [708.82, 1974.81]s + [2726.75, 3686.83].$$

For this values of k_d, k_p, and k_i closed loop poles location, closed-loop system response to 5% disturbance step, and Kharitonov rectangles are shown in Figs. 4(a), (b) and (c) respectively.

The heavy loading condition, P=1.0, Q=0.5, X=0.7 be the nominal operating point

$$G_{heavy}(s)\frac{-37.23s}{s^4 + 20.66s^3 + 168.69s^2 + 569.62s + 5798.4}$$

Repeating steps 2 to 5, we finally obtain: k_d =1.2020, k_p=14.3134, k_i=-94.5537.

By observing the pole locations in Fig. 5, we can say that the controller designed with nominal operating condition as heavy loading condition is not robust. It was already mentioned that CDM does not always guarantee robustness. To get the flexibility in choosing any operating point as our nominal operating condition, we include a pre-filter (Eq. 2) and search for the unknown parameters a & b by using GA such that the stability indices (standard CDM) are [2 2 … 2.5].

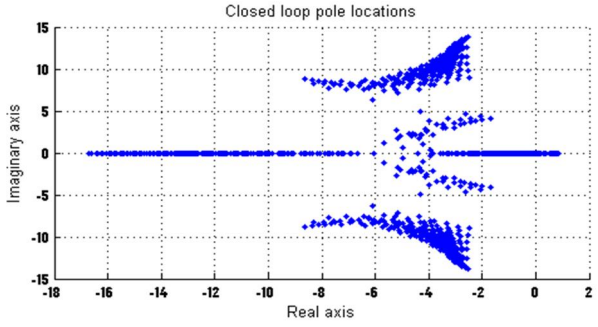

Fig. 5. Closed-loop poles location for the controller is not robustly stable.

This will give the robustness if the pole-zero pair is properly tuned. Out of 300 operating points we can choose anyone as the nominal operating point for designing the controller and we can attain robustness by proper tuning of pre-filter.

b) Fitness calculation for GA:

1. Using the nominal transfer function (with no perturbations), for a particular value of a and b (supplied by GA) find the values of k_d, k_p & k_i by using equations (18), (20) and characteristic polynomial. Find the roots of closed loop characteristic polynomial
2. By making perturbation in I_d, I_q and V obtain the open loop transfer function from equations mentioned in appendix. Find the closed loop transfer function, with the same controller designed at nominal operating point, which gives perturbed pole locations.
3. Using the pole coloring technique, calculate the distance between the corresponding nominal poles and the perturbed poles let sum of the distances be d_{ij} (distance corresponding to i^{th} pertubation and j^{th} iteration)
4. Repeat the steps 2 & 3 for 300 times, add all d'_{ij}s, $D_j = \sum_{i=1}^{300} d_{ij}$, $(D_j \; is \; to \; be \; minimised)$.

c) Robust for current control (PID and a pre-filter):

Step 1. Let the heavy loading condition P=1.0, Q=0.5, X=0.7, be the nominal operating point

$$G_{heavy}(s) = \frac{-37.23s}{s^4 + 20.66s^3 + 168.69s^2 + 569.62s + 5798.4}$$

Step 2. Choose controller to be designed as in Eq. (2)

Step 3. Obtain closed-loop Characteristic polynomial coefficients:

$$a_5 = 1;\; a_4 = 20.66 + b; a_3 20.66b + 168.69 + 37.23k_d$$
$$a_2 = 168.69b + 569.62 + 37.23ak_d + 37.23k_p$$
$$a_1 = 569.62b + 5798.4 + 37.23ak_p + 37.23k_i$$
$$a_0 = 5798.4b + 37.23ak_i$$

Step 4. Choose the stability indices according to the standard CDM as in Eq. (20)

Step 5. From equations (18), (20) and step3, we can get the values of k_d, k_p & k_i, for every given values of T_m and T_i. Using GA tune T_m and T_i by minimizing D_j.

k_d =2.93, k_p = 15.54, k_i = -36.23, T_m= 9.51, T_i= 11.36.

The interval characteristic polynomial of the closed loop system becomes:

$$G^{I}_{interval} = [1,1]s^5 + [32.02, 32.49]s^4 + [502.97, 605.57]s^3 + [5123.73, 5645.31]s^2 + [19024.95, 31328.33]s + [12350.93, 74198.11].$$

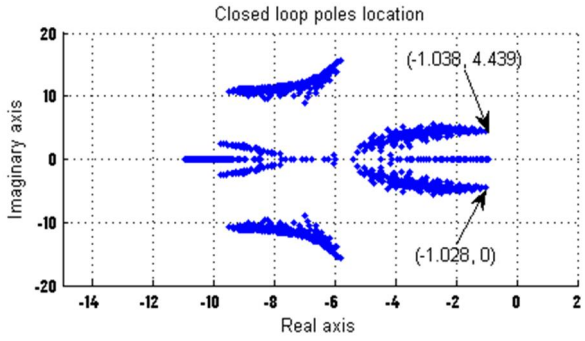

(a)

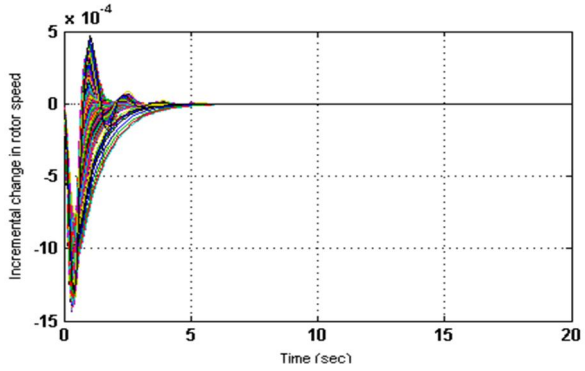

(b)

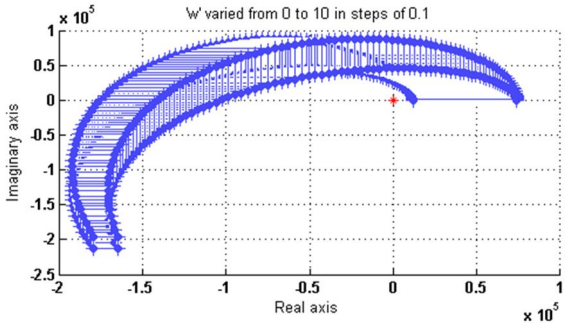

(c)

Fig. 6. (a) Closed-loop poles location. Most dominant pole is at -1.028, Minimum damping ratio offered is 13.16°; Closed loop system response to a 5% disturbance step at all 300 Operating points with k_d= 2.93, k_p= 15.54, k_i =-36.23, a = 9.51, b=11.36; (c) The Kharitonov Rectangles satisfying zero exclusion condition

Table 1. Robust current controller designed by choosing different operating points as nominal operating conditions

Loading condition: [Id, Iq, ω]	Controller [k_d, k_p, k_i, a, b]	Most dominant pole	Min. damping ratio (factor)
Normal: [0.7,0.15,0.45]	[3.08,15.60,-61.17,7.66,14.66]	-0.67	8.57° (0.15)
Heavy: [1.0,0.5,0.7]	[2.93,15.54,-36.23,9.51,11.36]	-1.03	13.16° (0.23)
Worst: [1.0,0.0,0.7]	[3.18,6.33,-45.38,10.81,12.15]	-0.71	9.61° (0.17)

In Table 1 we can find robust controller designed at different operating points (normal, heavy and worst loading conditions of a drive) as our nominal operating condition, which are satisfying all the closed loop requirements as mentioned in the problem.

In all the cases most dominant pole is always less than -0.5, and the minimum damping factor offered is always greater than 0.1. Thus the performance requirements are achieved.

4. SVM Technique for Three-Level Inverter

In multilevel voltage source inverters, SVM methodologies have the advantage of increased inverter output voltage. In this modulation technique as used in other works [38, 83], the space vector diagram of multilevel inverter is divided into different forms of sub-diagrams, in such a manner that the implementation becomes simpler. But these works do not reach a generalization of the two-level SVM because either they divided the diagram into triangles or interfered geometrical forms. In this work, a simple and fast method that divides the space vector diagram of three-level inverter into several small hexagons, each hexagon being space vector diagram of two-level inverter

4.1 Basic principle of SVM method

In this method, three-level inverter diagram is divided into six space vector diagrams of two level inverters. Thus the space vector modulation of three-level inverter becomes simple and similar to that of conventional two-level inverter space vector modulation. A three-level inverter space vector diagram and its six two-level hexagons are shown in Fig. 7. For each simplification, two steps have to be done so that three-level space vector plane is transformed to the two-level space vector plane.

1. From the location of a given reference voltage, one hexagon is selected among the hexagons.
2. Translate the origin of the reference voltage vector towards the centre of the selected hexagon.

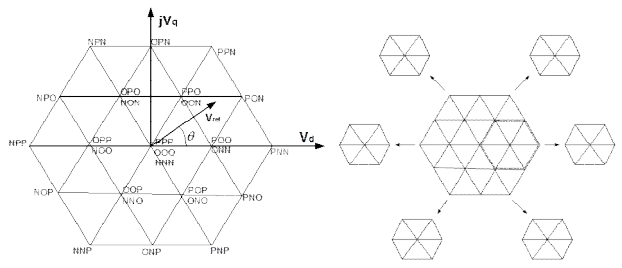

Fig. 7. Three-level inverter: (a) space Vector Diagram; (b) Decomposition of Space vector diagram

Then the determination of switching sequence and the calculation of the voltage vector duration time is done as in conventional two-level SVM method. As the proposed SVM method follows the same principle as that of conventional two-level SVM, various techniques used in two-level SVM can be applied to this proposed method.

4.2 Correction of reference voltage vector

By the location of a given reference voltage vector, one hexagon is selected among the six small hexagons that contains the three-level space vector diagram. This procedure divides the three-level space vector diagram into six regions. The value of S in Fig. 8 represents the Selection of hexagons which is based on phase angle θ of a reference voltage vector and its range is given in Table 2. In the Fig. 8, there exist some regions that are overlapped by two adjacent small hexagons in the three-level space vector diagram, so these regions are divided equally between the two hexagons and S can have multiple values.

Once the value of S is determined, the origin of a

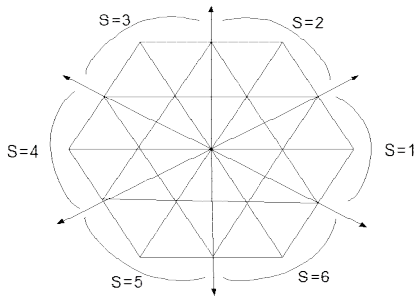

Fig. 8. Selection of Hexagon's Number

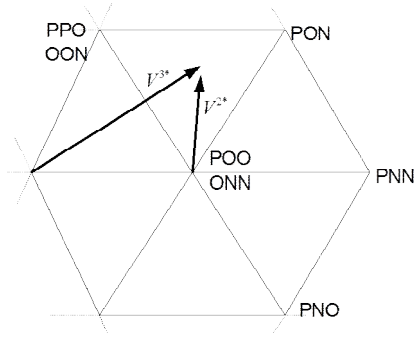

Fig. 9. Change of original reference voltage vector

Table 2. Selection of Hexagons based on Phase Angle θ of Reference Voltage Vector

S.NO	V^{2*}_d	V^{2*}_q
1	V^{3*}_d -2V.cos(0)	V^{3*}_d -2V.sin(0)
2	V^{3*}_d -2V.cos(π/3)	V^{3*}_d -2V.sin(π/3)
3	V^{3*}_d -2V.cos(2π/3)	V^{3*}_d -2V.sin(2π/3)
4	V^{3*}_d -2V.cos(π)	V^{3*}_d -2V.sin(π)
5	V^{3*}_d -2V.cos(4π/3)	V^{3*}_d -2V.sin(4π/3)
6	V^{3*}_d -2V.cos(5π/3)	V^{3*}_d -2V.sin(5π/3)

Table 3. Correction of Reference voltage vector (d and q components of the reference voltage V^{2*})

S.No.	Hexagon Number 'S'	Location of reference voltage vector phase angle θ
1.	1	$-\pi/6 < \theta < \pi/6$
2.	2	$\pi/6 < \theta < \pi/2$
3.	3	$\pi/2 < \theta < 5\pi/6$
4.	4	$5\pi/6 < \theta < 7\pi/6$
5.	5	$7\pi/6 < \theta < 3\pi/6$
6.	6	$3\pi/6 < \theta < 11\pi/6$

reference voltage vector is changed to the center voltage vector of the selected hexagon. This translation is done by subtracting the center vector of the selected hexagon from the original reference vector as shown in Fig. 9. Here V^{3*} is the original reference vector and V^{2*} is the corrected reference vector seen from the location (POO) and (OON). Table 3 gives the components d and q of the reference voltage V^{2*} after translation, for all the six hexagons. The index 2 and 3 indicates two and three-level cases respectively.

4.3 Determination of dwelling times

Once the corrected reference voltage V^{2*} and the corresponding hexagon is determined, we can use the conventional two-level SVM method to calculate dwelling times and switching pattern in the same manner as that of two-level SVM method. The only difference compared to two-level SVM is multiplication factor 2 appears in the calculation.

The effective times are calculated as

$$T_1 = \frac{2v^{2*}T_s}{v_{dc}\cdot\frac{2}{3}} \cdot \frac{\sin\left(\frac{\pi}{3}-\alpha\right)}{\sin\frac{\pi}{3}} \quad (25)$$

$$T_2 = \frac{2v^{2*}T_s}{v_{dc}\cdot\frac{2}{3}} \cdot \frac{\sin(\alpha)}{\sin\frac{\pi}{3}} \quad (26)$$

$$T_0 = T_s - T_1 - T_2 \quad (27)$$

4.4 Conversion of switching states

After calculating dwelling times, the switching sequence is to be determined. The switching sequence is determined on the basis of the center voltage vector of the selected hexagon, the switching sequence is determined as conventional two-level inverter. The switching sequence will be (POO)-(PON)-(OON)-(ONN). If the (ONN) vector is selected as a base and the notations used in two-level space vector diagram are adopted, the switching sequence can be expressed as (111)-(110)-(010)-(000). This switching sequence is exactly the same as that of conventional two-level SVM. The Conversion of Three-level Switching states to equivalent Switching states of Two-level space vector diagram depending on the S value.

5. Results and Discussion

The block diagram of the proposed indirect vector controlled induction motor drive with CDM-PI three-level inverter is as shown in Fig. 10. From the field control and speed control the reference values of currents i_{ds}^* and i_{qs}^* are obtained and these values are compared with the respective i_{d1} and i_{qs} currents generated by the trans-formation of phase currents with the unit vector. From the respective errors, d-axis voltage V_{ds} and q-axis voltage V_{qs} are generated through PI and CDM-PI controller. These voltages are then converted into stationary frame and then given to SVM block.

Simulation results are obtained under different conditions considering the reference value of speed as 1200 rpm and using the switching frequency 5 KHz. The performance induction motor parameters such as stator phase currents, torque and speed are obtained with three-level inverter controlled drives with PI controller are given in Figs. 11-15.

5.1 Performance during starting

The performance of the indirect vector controlled induction motor drive during the starting with conventional PI and CDM-PI with three-level inverter is shown Fig. 11(a) and 11(b). From these figures it is observed that the system with CDM-PI and three-level inverter reaches steady state early compared to conventional PI controlled drive. The maximum current during the starting is reduced with CDM-PI controller. Due to this decrease in current, air gap power increases and the electromagnetic torque increases. The maximum torque obtained with conventional PI is 12.5 and with CDM-PI 13.75., ie with the increase in the level starting torque is increased. The speed response also reaches steady state earlier with CDM-PI fed indirect vector controlled drive.

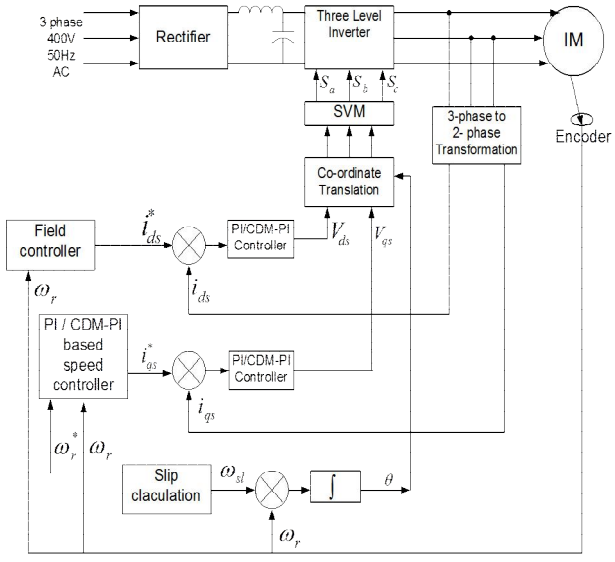

Fig. 10. Proposed vector control of induction motor

5.2 Performance during steady state

The steady state phase currents, torque and speed responses of indirect vector controlled drive with three-level are shown Fig. 12(a) and 12(b). It is observed that the torque ripple with conventional PI is 0.25 but with CDM-PI is only 0.03 because approximated three-level inverter output voltage contains less harmonic distortion. It is also observed that the speed response attains 1200 RPM value with CDM-PI but conventional PI is unable to attain the required value for the same DC link voltage 400V.

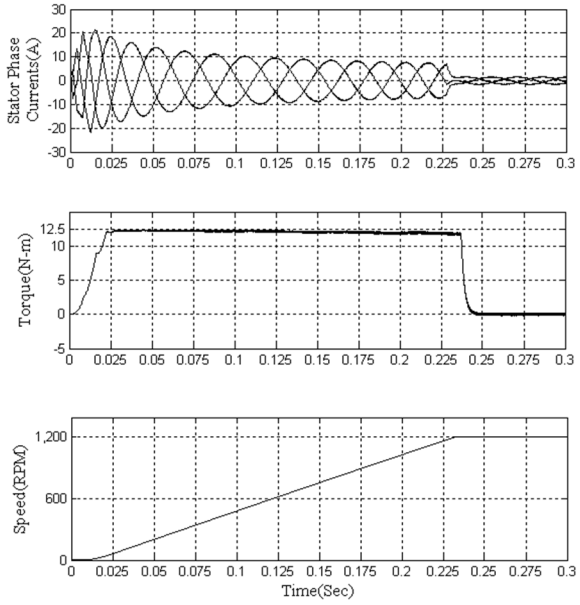

(a) With PI controller and three level inverter

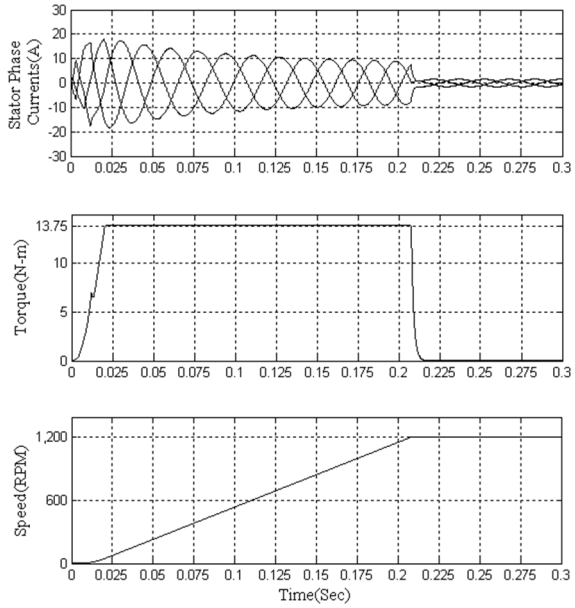

(b) With CDM-PI controller and three level inverter

Fig. 11. Performance of induction motor during starting

5.3 Performance during step change:

The response during the step change in load torque command (the load torque of 8 N-m is applied at 0.7 sec and removed at 0.9 sec) is shown in Figure 13(a) and 13(b). The ripple content in current waveforms and torque is less with CDM-PI indirect vector controlled induction motor drive. The momentary speed decrease less compared with conventional PI during the load change.

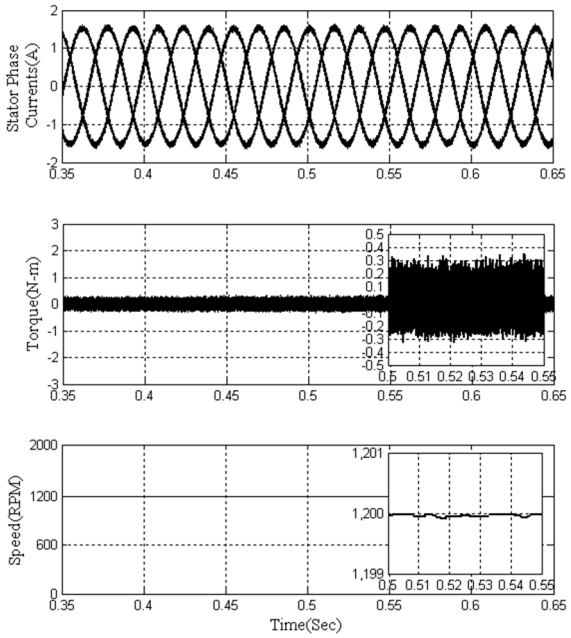

(a) With PI controller and three level inverter

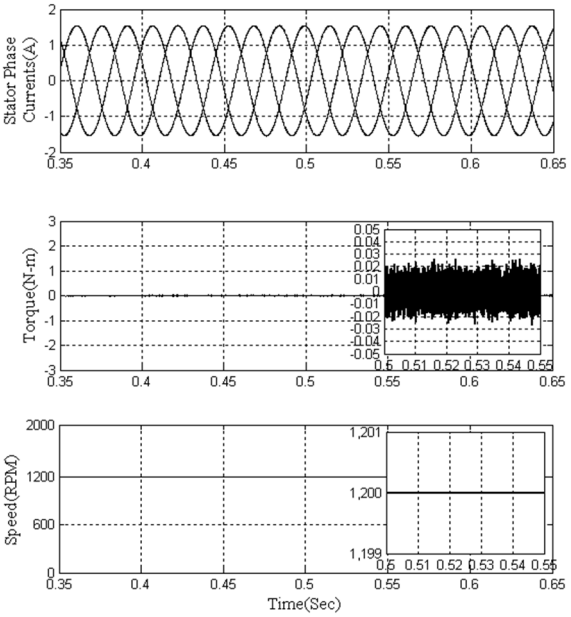

(b) With CDM-PI controller and three level inverter

Fig. 12. Steady state Performance of indirect vector controlled induction motor

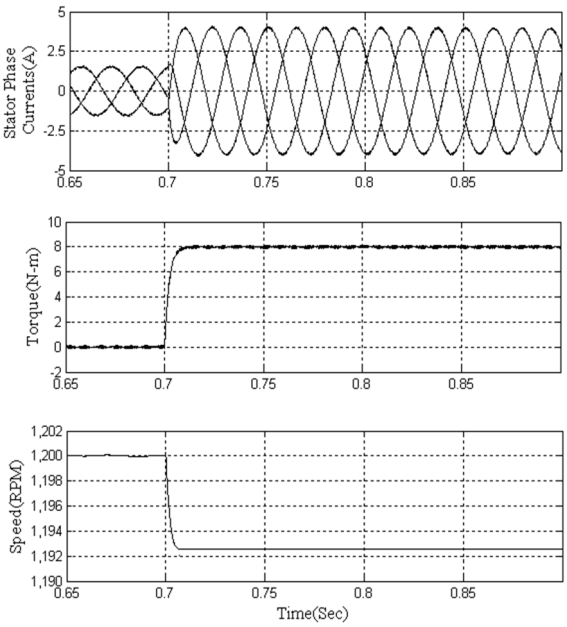

(a) With PI controller and three level inverter

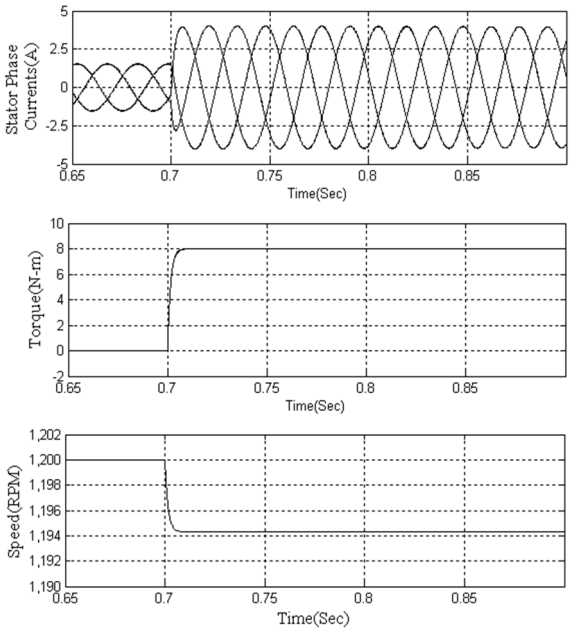

(b) With CDM-PI controller and three level inverter

Fig. 13. Performance of induction motor during step change in load torque

5.4 Performance during speed reversal:

The results of the drive during speed reversals (From +1200 to -1200 and vice versa) are shown in Figure 14(a) and 14(b). The drive gives less ripple content in the phase currents, torque of an induction motor and speed response reaches the reference value earlier time with CDM-PI with three-level inverter during the speed reversal.

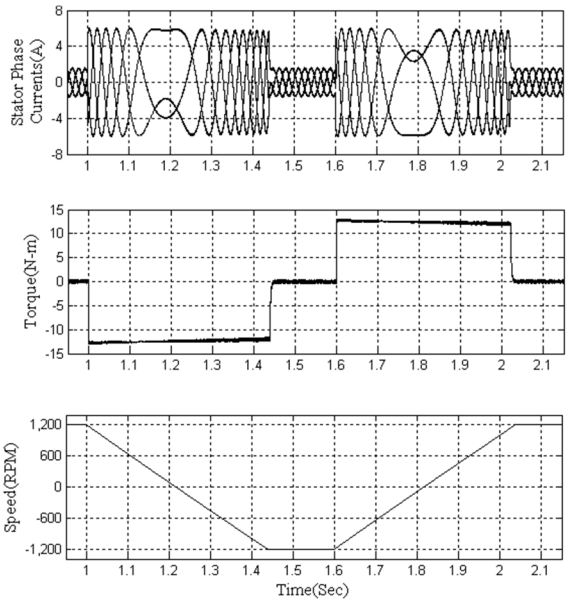

(a) With PI controller and three level inverter

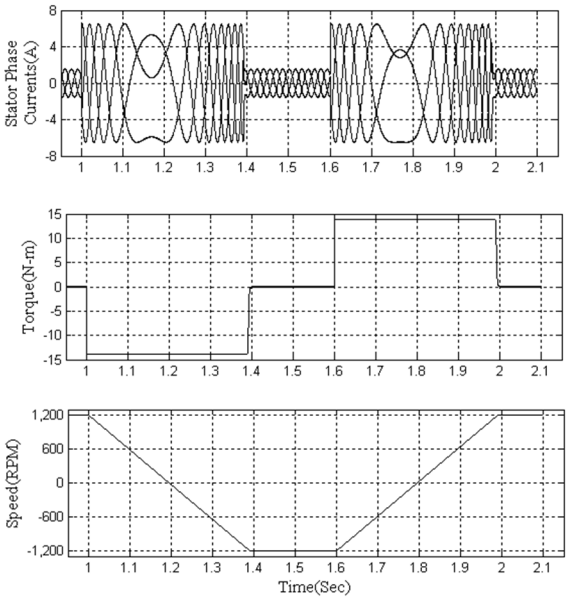

(b) With CDM-PI controller and three level inverter

Fig. 14. Performance during speed reversal (from +1200 rpm to -1200 rpm and from -1200 rpm to +1200 rpm)

6. Experimental Validation

A dSPACE (DS1103) is used for the real time implementation of vector controlled induction motor drive using the proposed and conventional PI Controller. The control algorithm is first developed in Matlab/Simulink. The real time workshop of Matlab generates the C code for the real time implementation. The interface between Matlab and DS1103 allows the controller to be run on the

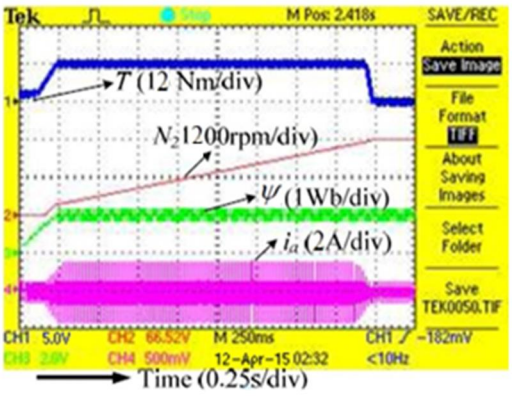

(a) With conventional PI controller

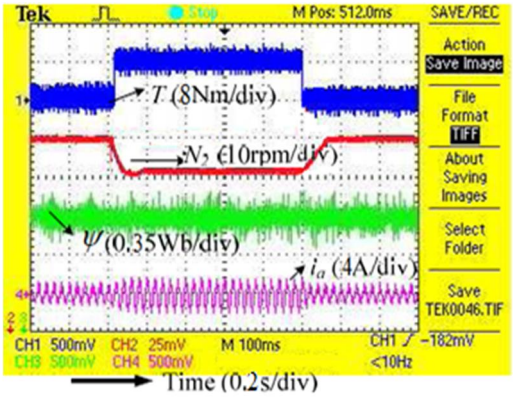

(a) With conventional PI controller

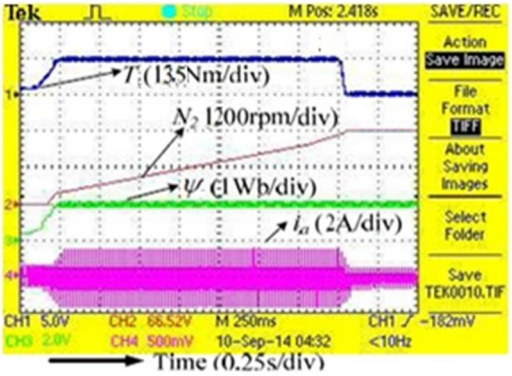

(b) With Co-Efficient diagram based PI controller

Fig. 15. Performance of vector controlled Induction motor

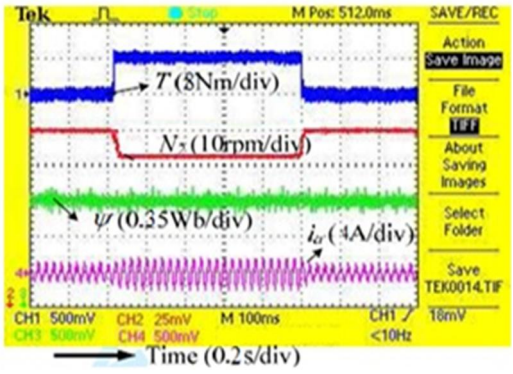

(b) With Co-Efficient diagram based PI controller

Fig. 16. Performance of Vector controlled Induction motor

hardware.

In the present case, the optimized C code of the simulink model of the control algorithm is automatically generated by the real time workshop of Matlab in conjunction with the dSPACE hardware, where it is implemented in the real time and the gating pulses are generated. The gating signals for the power switches of the inverter are outputted via the master bit I/Os are available on the dSPACE board. The CLP1103 Connector/Led Combination panel provides easy to use the connections between DS1103 board and the devices is to be connected to it. The panel also provides an array of LEDs indicating the states of digital signals (gating pulses). The gating pulses are fed to various IGBT driver circuits via the Opto-isolation circuit boards. Sensed signals fed to the ADCs and the generated gating pulses are outputted at master bit I/Os. The block diagram of dSPACE controlled inverter is shown in Fig. 12.

The schematic diagram gives the clear information of the experimental setup in detail. Here, the speed of the IM is sensed using DC-Vector control. In addition, currents, and the speed of IM are taken into the feedback using sensors via ADC and Mux ADC channels of the DSPACE DS-1103 connector panel. Thereafter, the speed and currents of the IM are estimated and given to the respective controllers. Moreover, the speed and current PI-controllers generate the current and slip speed

Initially, the reference speed set to 1200rpm in both conventional and proposed Co efficient diagram based PI controllers of the IM drive at no-load. The PWM pulses are provided to the inverter by a click on the incremental build. The DC-link voltage 500V is applied to the inverter by adjusting three-phase auto-transformer using uncontrolled rectifier. Hence, the IM picks up its speed up to required value, i.e., 600rpm and reach to steady state under no-load condition. The corresponding waveforms (torque (T_e), speed (N_r), flux (ψ_e), and current (i_a)) during starting for conventional are taken from the digital storage oscilloscope (DSO) as shown in Fig. 15(a & b) and Fig. 16(a & b).

6.1 Performance during starting

Compared to conventional PI Controller, the proposed co efficient diagram based PI controller has the better percentile ripple improvement in the induction motor parameters during its starting. Such as in torque it is 25%, in flux it is 25%, in current it is 18% and in speed it is about 8% ripple improvement.

6.2 Performance during Step change in load torque

A sudden load of 8N-m is applied/ removed at 0.4s and 0.9s then the corresponding changes in IM waveforms are

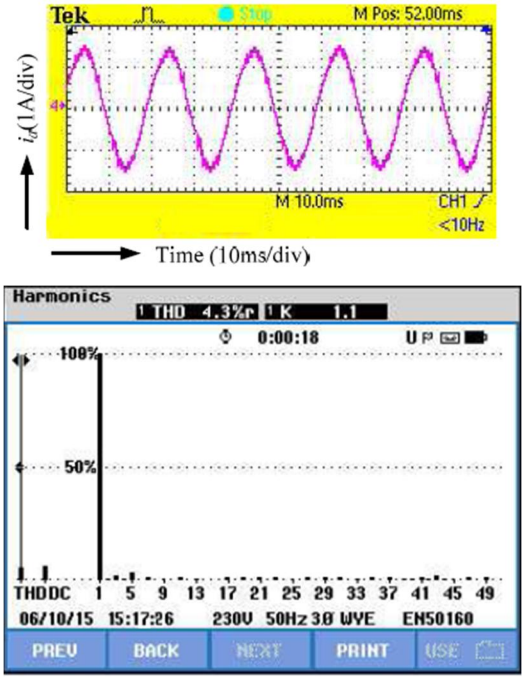

(a) With conventional PI controller

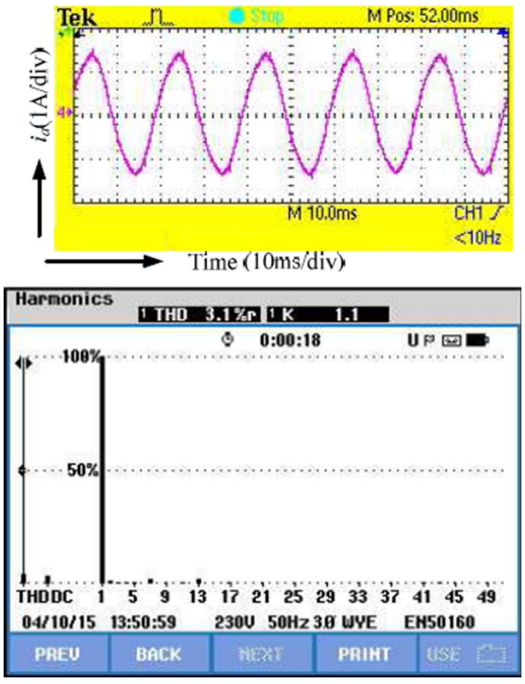

(b) With co efficient diagram based PI controller

Fig. 17. %THD of phase current

shown in Fig. 16(a) and 16(b). The torque and currents suddenly rise/fall due to load perturbation. The torque distortion, acceleration/deceleration of speed of IM at no load is 0.8N-m, and ±10rpm with conventional PI controlled system. But with Co-efficient diagram based PI controller torque distortion is 0.3 N-m and speed contains less variations

Table 4. THD comparison of phase current

Phase current	Three-level			
	PI controller		CDM- PI controller	
	Simulation	Experiment	Simulation	Experiment
I_{ph}	3.4	4.3	2.2	3.1

6.3 %THD comparison of phase currents

The steady state no-load current with conventional and Co efficient diagram based PI controlled system is 4.3% and 3.1% as shown in Fig. 17(a) and 17(b), respectively. The current THD is considerably less with Co efficient diagram based PI controlled system and hence the current THD performance is improved 27.9%

6.4 Comparison of THD :

The %THD values of three-level inverter fed induction motor drive phase current value with PI controller and Co efficient diagram based controller is given below in Table 4.

7. Conclusion

The performance indirect vector controlled induction motor drive is compared with Conventional PI and CDM-PI based Speed and current controllers using three-level inverter. The ripple content of stator phase currents, torque and oscillations in speed response are compared. The total harmonic distortion obtained in phase currents using CDM-PI based system is 30% less compared conventional PI controller fed indirect vector controlled induction motor drive. Using CDM robust controller can be designed by choosing any operating point (in the specified range) as our nominal operating condition. It is found that the induction motor has better performance with CDM-PI based controllers. The method is flexible to choose nominal operating point, where the motor is running most of the time, at which we desire better performance.

Appendix

Three-phase, 400 V, 1.3 hp, 1480 rpm induction motor
Parameters:
Stator resistance Rs = 4.1 Ω,
Stator inductance Ls=0.545 H,
Rotor resistance Rr = 2.5 Ω,
Rotor inductance Lr=0.542 H,
Mutual inductance Lm=0.51 H,
Moment of inertia J=0.04 Kg-m^2.

DC Link Voltage=500 V

References

[1] Toshiaki Murata, Takeshi Tsuchiya and Ikuo Takeda, "Vector Control for Induction Machine on the Application of Optimal Control Theory," *IEEE Trans. on Industrial Electronics*, vol. 37, no. 4, pp. 283-290, 1990.

[2] Yamamoto, S., and Hashimoto I., "Present status and future needs: the view from Japanese industry," *In proc. fourth int. conf. on chemical process control*, 1991.

[3] Wei-Der Chang, "A multi-crossover genetic approach to multivariable PID controllers tuning," *Expert Systems with Applications*, vol. 33, no. 3, pp. 620-626, 2007.

[4] Ya Gang Wang, and Hui He Shao, "Optimal tuning for PI controller," *Automatica*, vol. 36, no. 1, pp. 147-52, 2000.

[5] Herbert Werner, Petr Korba, and Tai Chen Yang., "Robust Tuning of Power System Stabilizers Using LMI-Techniques", *IEEE Trans. on Control Systems Technology*, vol. 11, no. 1, pp. 147-152, 2003.

[6] T. K Sunil Kumar and Jayanta Pal., "Robust tuning of power system stabilizers using Optimization Techniques", *IEEE international Conference*, pp. 1143-1148, 2006.

[7] Rao, P. S. and Sen, I., "Robust Tuning of Power System Stabilizers using QFT", *IEEE Trans. Control Systems Technology*, vol. 7, no. 4, pp. 478-486, 1999.

[8] M. T. Soylemez and N Munro, Robust Pole assignment in uncertain systems, Proc. IEE: Control Theory and Applications, vol.144, no.3, pp. 217-224, 1997.

[9] Li wang and Dinh-nhon Troung, "Stability Enhancement of DFIG based Offshore Wind Farm Fed to a Multi-machine System using STATCOM", *IEEE Transaction on power systems,* vol. 28, no. 3, pp. 2882-2889, 2013.

[10] Parag Kshirsagar, Jihoon Jang and Dushan Boroyevich "Implementation and sensorless vector-control design and tuning strategy for SMPM machines in fan type application", *IEEE Transaction on Industry Applications,* vol. 48, no. 6, pp. 2062-2069, 2012.

[11] Zhizheng Wu, Azhar Iqbal, and Foued Ben Amara, "LMI-Based Multivariable PID Controller Design and its Application to the Control of the Surface Shape of Magnetic Fluid Deformable Mirrors", *IEEE Transactions on Control Systems Technology*, vol. 19, no. 4, pp. 717-729, 2011.

[12] G. K. Singh, A. Senthil Kumar, and R. P. Saini, "Performance Analysis of a Simple Shunt and Series Compensated Six-phase Self-excited Induction Generator for Stand-alone Renewable Energy Generation", Energy Conversion and Management, vol. 52, no. 3, pp. 1688-1699, 2011.

[13] L. Ntogramatzidis and A. Ferrante "Exact tuning of PID controllers in control feedback design" IET Control Theory Appl., vol. 5, no. 4, pp. 565-578, 2011.

[14] M. Farahani S. Ganjefar M. Alizadeh "PID controller adjustment using chaotic optimization algorithm for multi-area load frequency control," *IET Control Theory,* vol. 6, no. 13, pp. 1984-1992, 2012.

[15] Kiyong Kim, Pranesh Rao and Jeffrey A. Burnworth, "Self-Tuning of the PID Controller for a Digital Excitation Control System", *IEEE Trans. on Industry Applications*, vol. 46, no. 4, pp. 1518-1524, 2010.

[16] V.P. Arikatla J.A.and Abu Qahouq, "Adaptive digital proportional integral derivative controller for power converters", *IET Power Electron*., vol. 5, no. 3, pp. 341-348, 2012.

[17] Srinivasan P, Narasimharaju. B. L, and Srikanth N. V, "Space vector pulse width modulation scheme for open end winding induction motor drive configuration", *IET Power Electronics,* vol. 8, no. 7, pp. 1083-1904, 2015.

[18] Durga Sukumar, Jayachandranath Jithendranatha and Suman Saranu, "Three-level Inverter-fed Induction Motor Drive Performance Improvement with Neuro-fuzzy Space Vector Modulation", *Electrical Power Component and Systems,* vol. 42, pp. 1633-1646, 2014.

[19] Narasimharaju B. L, S. P. Dubey and S. P. Singh, "Design and Analysis of coupled inductor Bi directional DC-DC converter for high voltage diversity applications", *IET Power Electronics,* vol. 5, no. 7, pp. 998-1007, 2012.

[20] C. Bharatiraja, Seenithangam Jeevananhan, Ramachandran Latha, V. Mohan, "Vector selection approach-based hexagonal hysteresis space vector current controller for a three phase diode clamped MLI with capacitor voltage balancing," *IEEE Transactions on IET Power Electronics*, vol. 9, no. 7, pp. 1350-1361, 2016.

[21] O. Bouhali, B. Francois, M. Berkouk and C. Saudemont, "DC Link Capacitor Voltage Balancing in a Three-Phase Diode Clamped Inverter Controlled by a Direct Space Vector of Line-Line Voltages," *IEEE Transactions on Power Electronics*, vol. 22, no. 5, pp. 1636-1648, 2007.

[22] P. J. Patel, Vinod Patel, P. N. Tekwani, " Pulse-based dead-time compensation method for self balancing space vector pulse width-modulated scheme used in three-level inverter-fed induction motor drive," *IEEE Transactions on IET Power Electronics*, vol. 4, no. 6, pp. 624-631, 2011.

[23] G. Durgasukumar and M. K. Pathak, "Comparison of adaptive Neuro-Fuzzy-based space-vectormodulation for two level inverter," *International Journal of Electrical Power & Energy Systems*, vol. 38, no. 1, pp. 9-19, 2012.

G. Durga Sukumar received bachelor and master degrees in Electrical Engineering from J.N.T.U, Hyderabad (India) and completed his Ph.D degree in the Electrical Engineering Dept, Indian Institute of Technology, Roorkee, India. He is presently working in Vignan Institute of Technology and Science, Yadadri Bhuvanagiri(Dist).His research interests include power electronics and electric drives, machines and new research eras in solar energy incorporated with type 2 / neuro fuzzy-based controllers.

T. Rama Subba Reddy, received bachelor, master degrees and Ph.D in Electrical Engineering from J.N.T.U, Hyderabad (India). He is presently working in Vignan Institute of Technology and Science, Yadadri Bhuvanagiri (Dist). His areas of interest include Reliability Evaluation and Redundancy Optimization of engineering systems and power system optimization.

B. Pakkiraiah received B. Tech degree in Electrical and Electronics Engineering, in 2010 and M. Tech degree in Power Electronics in 2013. He is presently pursuing Ph. D from Vignan's Foundation for Science Technology and Research University in the department of electrical and electronics engineering, with the specialization of power electronics and drives. His research interests are in power electronics and drives, neural networks and fuzzy logics and new research eras in renewable energy sources.